PCCP

Accepted Manuscript

ROYAL SOCIETY OF CHEMISTRY

www.rsc.org/pccp

Journal Name

RSCPublishing

ARTICLE

Iron-nitrogen-doped mesoporous tungsten carbide nanostructures as an oxygen reduction electrocatalyst

Cite this: DOI: 10.1039/x0xx00000x

Je-Suk Moon,[a] Young-Woo Lee,[a] Sang-Beom Han,[a] Da-Hee Kwak,[a] Kyung-Hoon Lee,[a] Ah-Reum Park,[a] Jung Inn Sohn,[b] Seung Nam Cha[b] and Kyung-Won Park*[a]

Received 00th January 2012,
Accepted 00th January 2012

DOI: 10.1039/x0xx00000x

www.rsc.org/

Since Pt-based catalysts have disadvantages of high cost, large overpotential loss, and limited long-term stability, there have been various promising alternatives to Pt-based catalysts to improve the catalytic activity toward oxygen reduction reaction (ORR). We have synthesized iron-nitrogen-doped mesoporous tungsten carbide catalysts (WC-m-FT) pyrolyzed by the well-ordered mesoporous tungsten carbides with porphyrinic iron. The WC-m-FT exhibits an excellent ORR catalytic activity in alkaline medium, *i.e.* high electron-transfer number, as well as superior stability and methanol tolerance. The improved activity and stability of the WC-m-FT are ascribed to iron-containing catalytic active sites surrounded by nitrogen species and well-defined mesoporous tungsten carbide structure.

Introduction

Since oxygen reduction reaction (ORR) exhibits sluggish kinetics of molecular oxygen in low-temperature fuel cells, platinum-based materials are well known to be utilized as the most active ORR catalysts in the cathode.[1-3] However, Pt-based catalysts have disadvantages of high cost, large overpotential loss, and limited long-term stability.[4-6] Currently, there have been a variety of promising candidates for alternating Pt catalyst such as nitrogen-doped carbon nanotubes or graphene, and various metal-N_4 chelate macrocycles to enhance ORR activities.[7-20] In particular, carbon supported transition metal-N_4 chelate macrocycles such as metal phthalocyanines and metal porphyrins have been intensively investigated as promising non-Pt catalysts since the work of Jasinski in 1964.[21-25] Li *et al.* reported that iron and nitrogen doped carbon nanotube-graphene complex showed a high ORR activity and superior stability in both acid and alkaline solution.[14] Wu *et al.* represented polyaniline (PANI)-metal-C catalysts for promising ORR activity.[26] The PANI-Fe-C and PANI-FeCo catalysts exhibited high ORR activities in acid medium. Jiang *et al.* studied that the graphene-iron phthalocyanine composite catalyst exhibits comparable activity, superior stability, and methanol tolerance in alkaline solution.[25] Fu *et al.* reported the transition metal nitrogen containing moieties ($M–N_x$, M = Fe or/and Co, x = 2 or 4) embedded into the graphene sheets that exhibit high ORR properties in alkaline medium.[27] The active sites of these compounds are the four nitrogen ring coupled with transition metals, commonly Fe or Co, representing four-electron transfer process and highly selective catalytic activity for ORR.[28-33]

Furthermore, there have been many efforts to enhance ORR catalytic activity and stability using particular supporting materials such as transition metal oxides and carbides, because of stability of oxides and catalytic properties of carbides.[34-37] In particular, for transition metal carbides to mimic the catalytic properties of Pt-group metals, Levy and Boudart proposed that tungsten carbide (WC) displayed Pt-like behavior in catalytic reactions, which have a similar electronic density to Pt and exhibit a comparable catalytic activity in ORR.[38] Although the catalytic activity of WC is still lower than that of noble metals, a considerable interest has been received in fuel cells for the development of inexpensive systems. Recently, to solve limitation of electrochemical activity of tungsten carbide in ORR, there are many literatures for the controlled specific surface area, noble metals deposited on tungsten carbides, and tungsten carbide-based composite nanostructures.[39-43]

Here, we prepared iron-nitrogen-doped well-defined mesoporous tungsten carbides as a cathode catalyst by means of template-free synthesis. The iron-nitrogen-doped well-defined mesoporous tungsten carbides were characterized by field-emission scanning electron microscopy (FE-SEM), field-emission transmission electron microscopy (FE-TEM), X-ray powder diffraction (XRD), X-ray photoelectron spectroscopy (XPS), and Raman spectrometer. The surface area and porosity of the synthesized samples were analyzed by a nitrogen sorption measurement. To evaluate the performance of the catalysts for ORR, cyclic voltammograms (CVs) and linear sweep voltammograms were obtained in comparison with Pt/C catalyst using a potentiostat.

Experimental

Synthesis of mesoporous tungsten carbide based catalysts.

To prepare layered tungsten nitride nanoparticles, layered tungsten oxide was prepared by a hydrothermal method. For the layered tungsten oxide particles, ammonium tungstate ($(NH_4)_{10}H_2(W_2O_7)_6$) (Aldrich, 99.99%) as a precursor was dissolved in 5 M hydrochloric acid solution (Aldrich, 35%) with constant stirring at 25 ^oC for 1 h and then kept at 140 ^oC for 2 h. After the hydrothermal process, the resulting precipitate was cooled to room temperature, washed several times with ethanol and distilled water, and then filtered by using a filtration. The yellow layered tungsten oxide powder was obtained after drying in 50 ^oC oven. For tungsten nitride

structures from tungsten oxides, the resulting powder was loaded into a quartz boat, which was inserted into a vitreous quartz tube inside a cylindrical furnace, heated to reaction temperatures until 700 °C for 1 h, and then maintained at 700 °C for 3 h under NH_3 flow of 100 mL min^{-1}. The samples were cooled down to room temperature by flowing NH_3, and passivated for 2 h in an air flow in order to avoid drastic reoxidation to tungsten oxide when they were exposed to air. The as-prepared tungsten nitrides were then loaded into a quartz boat, which was then inserted into a vitreous quartz tube inside a cylindrical furnace. A gas mixture of 25% CH_4/H_2 was passed through the quartz tube at a rate of 100 mL min^{-1} during the entire reaction. Tungsten carbide catalysts studied in this work were prepared at 900 °C (denoted as WC-m). After carburization, all the samples were passivated in an air gas flow for more than 5 h before being removed from quartz tube.

The nitrogen-doped mesoporous tungsten carbide catalysts (denoted as WC-m-T) were prepared as follows: the WC-m powder was mixed with 5,10,15,20-Tetrakis(4-methoxyphenyl) -21*H*,23*H*-porphyrin (TMPP) solution (dissolved in 99.7% acetic acid (Aldrich) solution) for 1 h. For iron-nitrogen-doped mesoporous tungsten carbide catalysts (denoted as WC-m-FT), 5,10,15,20-Tetrakis(4-methoxyphenyl)-21*H*,23*H*-porphine iron(III) chloride (Fe-TMPP, 0.1 g, Aldrich) were dissolve in 99.7% acetic acid (Aldrich) solution for 1 h and mixed with the WC-m. Under vigorous stirring, the mixed solutions were completely evaporated the solvent at 70 °C and then dried in 50 °C oven at overnight. The obtained powders were placed in a quartz boat and pyrolyzed at 700 °C for 3 h (denoted as WC-m-T and WC-m-FT, respectively).

Electrochemical properties of the catalysts were measured in a three-electrode cell at 25 °C using a potentiostat (CH Instrument, CHI 700C). Pt wire and Hg/HgO (in saturated NaOH) were used as a counter and reference electrode, respectively. The rotating disk electrode as a working electrode was polished with 1, 0.3, and 0.05 μm Al_2O_3 paste and then washed in deionized water. The catalyst inks were prepared by ultrasonically dispersing catalyst powders in an appropriate amount of Millipore water and ethanol. The catalyst ink was dropped 0.9 μL onto a rotating disk electrode (0.126 cm^2). After drying at 50 °C oven, the total loading of all catalysts was 400 μg cm^{-2}. To compare electrochemical properties and ORR activity of the catalysts, CVs and linear sweep voltammetric curves were obtained in 0.1 M NaOH solution. The stability test was carried out by applying between -0.4 and +0.1 V for 2,000 cycles with a scan rate of 50 mV s^{-1} in O_2-saturated 0.1 M NaOH solution at 25 °C. The oxygen reduction current–potential curves before and after the stability test of the catalysts were obtained by sweeping the potential from -0.9 to 0.3 V at a scan rate of 5 mV s^{-1} and rotation disk speed of 1600 rpm. Methanol-tolerance ORR activity of the catalysts was obtained in O_2-saturated 0.1 M NaOH with 0.5 M CH_3OH solution. To determine the role of iron in the ORR active sites in the catalysts, the ORR polarization curves for the samples were obtained in O_2-saturated 0.1 M NaOH with CN^-.

Structural and electrochemical characterization of as-prepared catalysts.

The as-prepared samples were characterized by FE-TEM and energy dispersive X-ray (EDX) spectroscopy using a Philips, Tecnai F20 system operating at 200 kV. The TEM samples were prepared by placing a drop of the nanoparticle suspension in ethanol on a carbon-coated copper grid. FE-SEM image was obtained on a Carl Zeiss, SIGMA microscope operating at 5 kV. Structural analysis of the mesoporous structures was carried out by XRD method using a Bruker, D2 Phase System equipped with a Cu K_α radiation source of λ = 0.15406 nm with a Ni filter. The tube current was 10 mA with a tube voltage of 30 kV. The 2θ between 20° and 80° was explored at a scan rate of 5° min^{-1}. Raman spectra were recorded on High Resolution Micro Raman spectrometer (Horiba Jobin Yvon, LabRAM HR UV/Vis/NIR PL). XPS (Thermo Scientific, K-Alpha) analysis was carried out with the Al K_α X-ray source of 1486.8 eV at the chamber pressure below 1 x 10^{-8} Torr and 200 W beam powers. All high resolution spectra were collected using pass energy of 46.95 eV. The XPS samples were prepared by mixing with Sn metal for making pellet. The surface area and porosity of the as-synthesized samples were analyzed by a nitrogen sorption measurement (Micromeritics ASAP 2020 adsorption analyzer).

Results and discussion

Fig. 1 shows TEM and SEM images of as-prepared WC-m, WC-m-T and WC-m-FT. The as-prepared samples exhibit porous structure with fairly uniform and regular mesopores. In our previous study, well-defined mesoporous tungsten nitride was synthesized by means of a template-free synthetic approach.[44] In particular, during nitridation process using layered tungsten oxide, the tungsten nitride was gradually reduced and then the homogeneous substitution of oxygen vacancies in the reduced oxides with nitrogen atoms occurred.

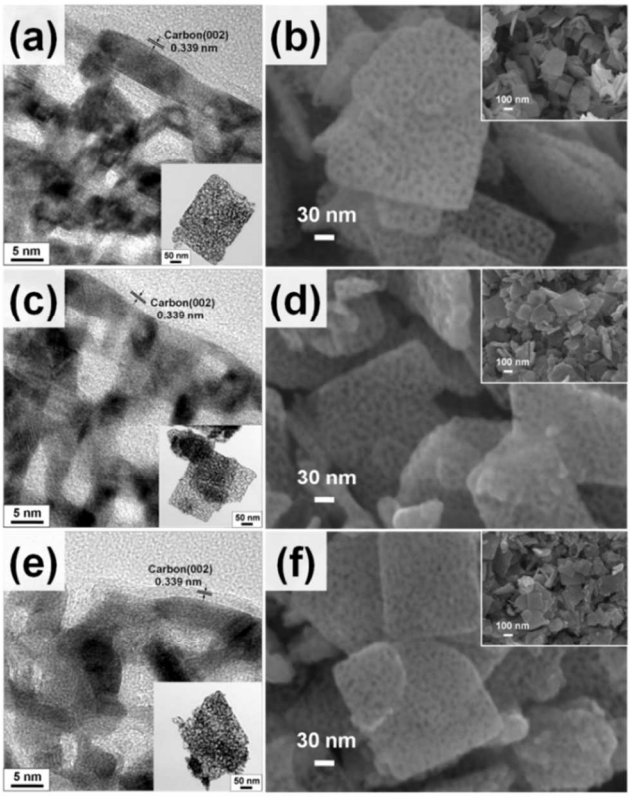

Fig. 1 HR-TEM images of (a) WC-m, (c) WC-m-T, and (e) WC-m-FT (The insets indicate the FE-TEM images). HR-SEM images of (b) WC-m, (d) WC-m-T, and (f) WC-m-FT (The insets indicate the FE-SEM images).

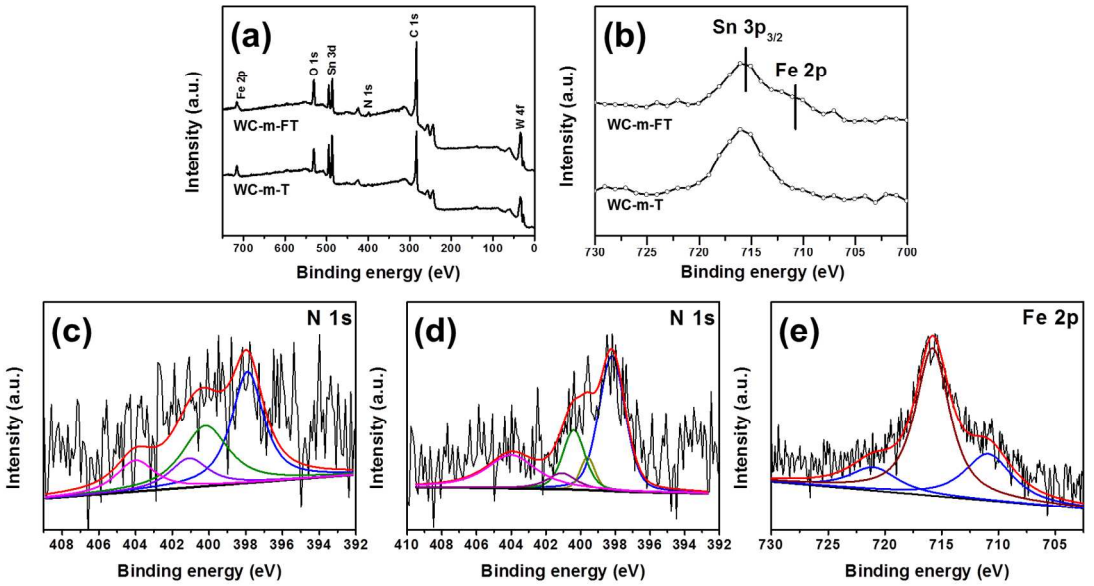

Fig. 2 (a) XPS survey spectra of WC-m-TF and WC-m-T. (b) XPS spectra between 700 and 730 eV of WC-m-TF and WC-m-T. N1s XPS spectra of (c) WC-m-T and (d) WC-m-FT. (e) Fe2p XPS spectrum of WC-m-FT.

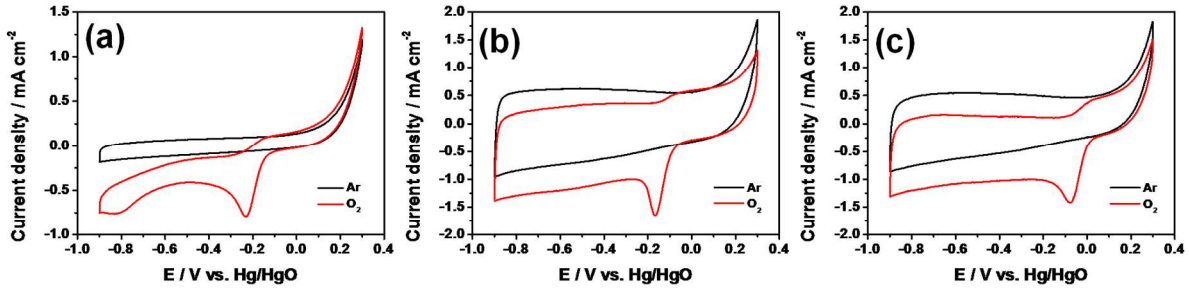

Fig. 3 CVs of (a) WC-m, (b) WC-m-T, and (c) WC-m-FT in Ar- or O_2-saturated 0.1 M NaOH with a scan rate of 50 mV s^{-1} at room temperature.

The layered tungsten oxide can offer more open sites forming mesoporous structure. During the carburization process of the mesoporous tungsten nitride, it is found that the tungsten nitride is gradually carburized due to homogeneous substitution of nitrogen atoms in the metal nitride with carbon atoms without serious collapse and aggregation. The as-prepared WC-m, WC-m-T and WC-m-FT show well-defined porous structures with mesopores of 5~12 nm in diameter. Furthermore, as shown in the FE-TEM images (Fig. 1a,c,e), WC-m, WC-m-T and WC-m-FT represent carbon shell layers (1.9~2.2 nm in thickness) having the {002} facet with the *d*-spacing of 0.339 nm of graphitic layers, which is similar to {002} facet with *d*-spacing of 0.335 nm of typical graphite.[45] The feasible formation process of the mesoporous tungsten carbides coated by carbon layers under CH_4 atmosphere is as follows:

$$W_2N + CH_4 \rightarrow \text{WC-m} + CH_4$$
$$\rightarrow \text{WC-m} + C_{ad} + 2H_2 \rightarrow \text{WC-m@C} \quad (1)$$

As shown in Raman spectra of WC-m, WC-m-T and WC-m-FT (Fig. S1), the two peaks are attributed to G band at 1584 cm^{-1} and D band at 1350 cm^{-1}, respectively. The G band was related to the E_{2g} vibration mode of sp^2 carbon structures. The D band is related to structural defects and partially disordered structures on the graphitic plane, which are caused by heteroatom (nitrogen or oxygen) doping.[46-47] The intensity ratio (I_D/I_G) values of WC-m, WC-m-T, and WC-m-FT are 1.11, 1.18 and 1.19, respectively. The increased I_D/I_G was attributed to the structural defects caused by pyrolyzed with TMPP and Fe- TMPP as precursors, namely nitrogen or iron-nitrogen doping.

XPS analysis was performed to analyze the content and chemical state of the elements in the catalysts. The XPS survey spectra for WC-m-T and WC-m-FT displayed the presence of W, C, and N on the catalyst surfaces (Fig. 2a). As shown in Fig. S2a, tungsten species of WC-m-T contain $W4f_{7/2}$ at 32.2 eV and $W4f_{5/2}$ at 34.4 eV, indicating that tungsten species are formed during the carbide formation, with $W4f_{7/2}$ at 35.8 eV and $W4f_{5/2}$ at 38 eV related to WO_3.[48] In Fig. S2b, three peaks at 284.6, 286.2 and 288.5 eV, which are assigned to the carbon component of WC-m-T in C-C, C-O and O=C-O, respectively.[11] By combining data of C1s and W4f spectra, the surface state WC-m almost consists of a carbide state. Also, WC-m-T and WC-m-FT contain pyridinic, pyrrolic, graphitic, and oxidated nitrogen species with a nominal nitrogen level of ~4.47 and ~2.26 at%, respectively (Fig. 2c,d). The high-resolution N1s spectra of the as-prepared samples were fitted with several different signals having binding energies of 398.3, 400.1, 401.4, 403.7 eV, corresponding to pyridinic N, pyrrolic N, graphitic N, and oxidated N, respectively.[49] Nitrogen groups

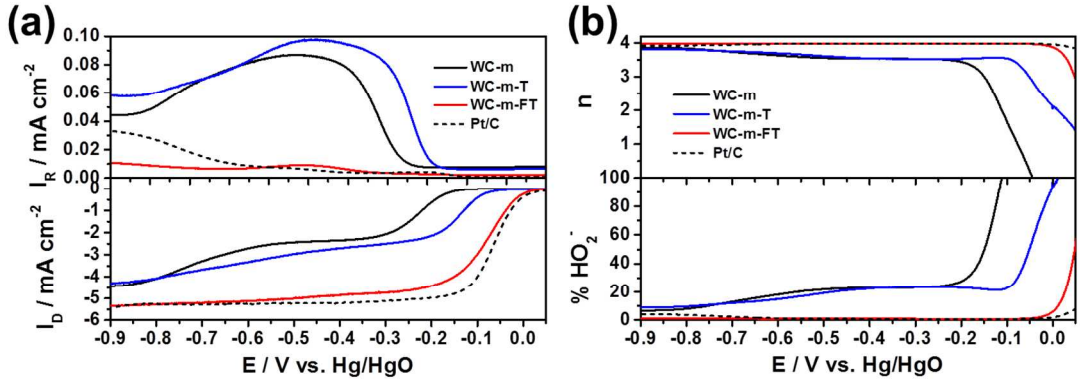

Fig. 4 (a) RRDE polarization curves of WC-m, WC-m-T, and WC-m-FT in O_2-saturated 0.1 M NaOH with a scan rate of 5 mV s^{-1} and an electrode rotation rate of 1600 rpm at room temperature. The ring potential was maintained at 0.15 V *vs* Hg/HgO. (b) Electron-transfer number and $\%HO_2^-$ of the as-prepared samples for ORR.

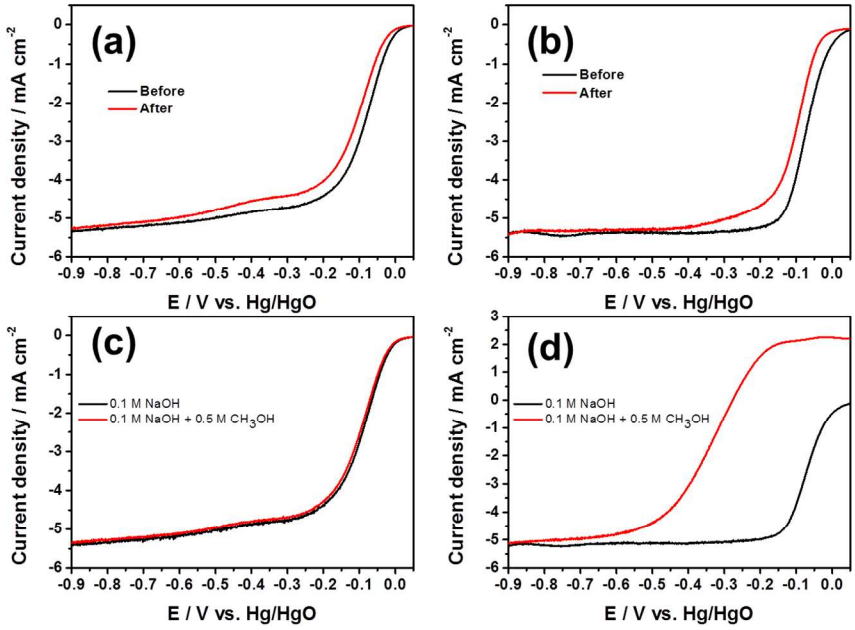

Fig. 5 Polarization curves of (a) WC-m-FT and (b) Pt/C before and after stability in O_2-saturated 0.1 M NaOH solution with a scan rate of 5 mV s^{-1} and an electrode rotation rate of 1600 rpm at room temperature. Polarization curves of (c) WC-m-FT and (d) Pt/C with a scan rate of 5 mV s^{-1} and an electrode rotation rate of 1600 rpm in O_2-saturated 0.1 M NaOH solution with or without 0.5 M CH_3OH.

in WC-m-T and WC-m-FT result from pyrolyzing with TMPP and Fe-TMPP. In particular, the peak at 399.8 eV might also contain a contribution from nitrogen-bound metal (referred as here Fe-N).[50] The pyridinic N, Fe-N, and graphitic N are typically believed to participate in the active sites for ORR.[24,25] In Fig. 2e, Fe2p XPS spectra of WC-m-FT consist of $Fe2p_{3/2}$ at 710.9 eV and $Fe2p_{1/2}$ at 721 eV. The $Fe2p_{3/2}$ spectrum of WC-m-FT consist of metallic and oxidation states of iron with binding energies of 707.5, 709.4 and 710.9 eV, corresponding to Fe or Fe-C, Fe^{2+} and Fe^{3+} respectively.[51,52] In particular, the amount of Fe species in WC-m-FT is 1.77 at%.

Fig. S3 shows XRD patterns of WC-m, WC-m-T and WC-m-FT. The diffraction patterns of the as-prepared WC-m are related to the mixed phase of both WC_{1-x} with a face-centered cubic (fcc) lattice (JCPDS No. 20-1316) and WC with a hexagonal closed packing (hcp) lattice (JCPDS No. 65-4539). WC-m-T and WC-m-FT shows the mixed phase consisting of fcc WC_{1-x} and hcp WC, representing that the samples pyrolyzed with TMPP and Fe-TMPP as precursors have the same crystal structure as that of the WC-m. To characterize pore structure of the samples, curves of nitrogen gas adsorption-desorption isotherm and pore size distribution were obtained (Fig. S4a). WC-m shows fairly uniform pore sizes of ~10.97 nm, which are indicative of mesoporous structure, and specific surface areas of ~47.85 m^2 g^{-1}.

CVs of the samples in Ar- and O_2-saturated 0.1 M NaOH were obtained to evaluate ORR properties of the samples in alkaline solution (Fig. 3). The oxygen reduction peak potentials of WC-m, WC-m-T, and WC-m-FT in O_2- saturated 0.1 M NaOH are -0.231, -0.164, and -0.076 V, respectively. The reduction peaks of WC-m, WC-m-T, and WC-m-FT are shifted into more positive potential in the CVs. The reduction peak potential of WC-m-FT toward ORR in the polarization curves is significantly shifted to positive direction as compared to WC-m and WC-m-T.

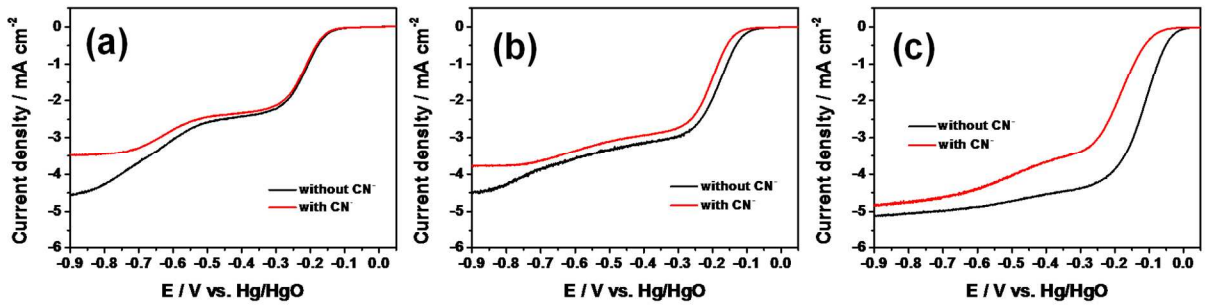

Fig. 6 Polarization curves for (a) WC-m, (b) WC-m-T, and (c) WC-m-FT with a scan rate of 5 mV s^{-1} and an electrode rotation rate of 1600 rpm in O_2-saturated 0.1 M NaOH solution with or without 10 mM KCN at 25 °C.

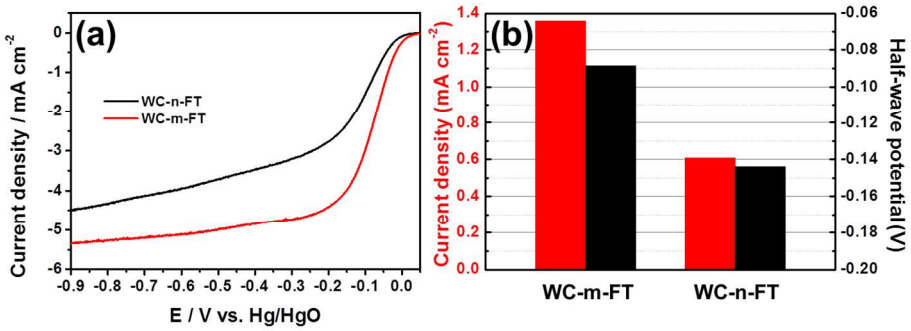

Fig. 7 (a) Polarization curves of WC-m-FT and WC-n-FT in O_2-saturated 0.1 M NaOH with a potential scan rate of 5 mV s^{-1} and an electrode rotation rate of 1600 rpm. (b) Comparison of current density at -0.05 V and half-wave potentials of the WC-m-FT and WC-n-FT.

To further characterize ORR properties of the samples in alkaline solution, rotating ring-disk electrode (RRDE) polarization curves of the samples in O_2-saturated 0.1 M NaOH solution were obtained as shown in Fig. 4. For comparison, commercial Pt catalyst (20 wt%) on Vulcan carbon black (Pt/C) was utilized. The disk current density(I_D) of WC-m-FT is much larger than those of WC-m and WC-m-T, whereas the ring current density(I_R) of WC-m-FT is comparably smaller than those of WC-m and WC-m-T. WC-m-FT exhibits an excellent ORR activity *i.e.* more positive onset potential (~0.05 V) and more positive half-wave potential ($E_{1/2}$ ~-0.088 V) compared to WC-m and WC-m-T (Fig. 4a). The plots of electron-transfer number (*n*) and generation yield of hydrogen peroxide (% HO_2^-) during ORR *vs*. electrode potentials are shown in Fig. 4b. The *n* and % HO_2^- can be obtained according to the following equations:

$$n = \frac{4i_d}{i_d + i_r / N} \quad (2)$$

$$\%\,HO_2^- = \frac{4-n}{2} \quad (3)$$

where i_d is the current on glass carbon electrode, i_r is the current on ring disk electrode, and N is the collecting coefficient number of -0.4245. The *n* exchanged by WC-m-FT toward ORR at all potentials is determined to be ~3.97 *i.e.* almost four electron transfer process as compared with WC-m and WC-m-T. The WC-m-FT exhibits much lower % HO_2^- yield at all potentials in comparison with WC-m and WC-m-T. Thus, WC-m-FT displays remarkably enhanced ORR activity, approaching that of Pt/C, with the n of ~4 and extremely low % HO_2^- yield during the ORR in alkaline solution. The stability test of the samples was performed by cycling the catalysts between -0.4 and 0.1 V at 50 mV s^{-1} in O_2-saturated 0.1 M NaOH. After 2000 cycling test in O_2 atmosphere, the half-wave potential of WC-m-FT exhibits a slight negative shift (~23.9 mV) as compared to Pt/C (~29.2 mV). (Fig. 5a,b). In direct methanol fuel cells, the tolerance of ORR catalysts to the CH_3OH molecule as a fuel that might pass through the polymer electrolyte membrane from anode side should be remarkably required. Compared to the RRDE curves in the presence of 0.5 M CH_3OH, Pt/C exhibits a serious decrease for the ORR performance, whereas WC-m-FT displays a slight ORR activity loss, thus representing an excellent tolerance of the catalyst to methanol poisoning effect (Fig. 5c,d).

To determine the role of iron as an active catalytic site for ORR in WC-m-FT, the ORR activity of WC-m-FT and WC-m-T was compared in O_2-saturated 0.1 M NaOH with or without 10 mM KCN (Fig. 6). Especially, it has been known that CN^- ions coordinate to iron, thus resulting in poisoning iron active sites toward ORR.[53] WC-m-FT exhibits a significantly deteriorated ORR activity, *i.e.* more negative shift of the ORR potential and decreased diffusion-limiting current, resulting from the diminished catalytic active sites due to blocking of the iron sites by CN^- ions. In contrast, WC-m-T with the nitrogen functionalities is found to show less ORR activity loss in O_2-saturated 0.1 M NaOH with or without CN^-. This suggests that both iron and nitrogen species in the catalysts are the crucial sites for ORR catalytic activity.

To investigate the effect of pore structure in tungsten carbide on the ORR activity, the sample (denoted as WC-n) was prepared by commercial tungsten oxide powder heated at 900 °C in CH_4/H_2. WC-n exhibits non-porous structure and low specific surface area of ~8.536 m^2 g^{-1} in comparison with the well-defined mesoporous WC-m (Fig. S4b). In particular, WC-m having a well-defined mesoporous structure displays excellent ORR activity and stability compared to the WC-n (Fig. S5). Additionally, WC-m shows a higher limiting current

density between -0.3 and -0.9 V, resulting from the access to large active sites and improved mass transporting as a result of the mesoporous structure of WC-m. The sample pyrolyzed with Fe-TMPP on WC-n (denoted as WC-n-FT) displays the diffraction patterns related to an hcp structure containing Fe component of 0.88 at% (Fig. S6). The onset potential of WC-n-FT toward ORR in the RRDE curves is similar to WC-m-FT (Fig. 7a). However, WC-m-FT shows an excellent ORR activity, *i.e.* higher kinetic and diffusion-limiting currents compared to WC-n-FT. The current density of WC-m-FT and WC-n-FT are 1.36 and 0.61 mA cm^{-2}, respectively, at -0.05 V, *i.e.* the kinetic controlled region. Also, WC-m-FT exhibits higher a half-wave potential (-0.088 V) in comparison with WC-n-FT (-0.144 V). The higher kinetic current density of WC-m-FT is ascribed to much higher active sites on the high surface area of WC-m. Furthermore, the well-ordered mesoporous structure of WC-m-FT can lead to higher diffusion-limiting current density. After cycling stablity test, the ORR activity of WC-n-FT displays a serious loss (Fig. S7), representing the sufficient active sites in the surface layers compared to WC-m-FT, the active sites might be widely distributed in the sample.

Conclusions

In summary, we have synthesized iron-nitrogen-doped mesoporous tungsten carbide catalysts with iron coordinated by pyridinic nitrogen atoms. WC-m-FT exhibits high ORR catalytic activity, improved electron-transfer number, methanol tolerance, and excellent stability in alkaline medium. The excellent activity and stability of WC-m-FT are ascribed to iron-containing catalytic sites surrounded by nitrogen species and mesoporous tungsten carbide structure.

Acknowledgement

This work was supported by the National Research Foundation of Korea Grant funded by the Korean Government (NRF-2011-0030335).

Notes and references

[a]Department of Chemical Engineering, Soongsil University, Seoul 156743, Republic of Korea. *E-mail: kwpark@ssu.ac.kr (Prof. K.-W. Park); Tel: +82-2-820-0613; Fax: +82-2-812-5378.
[b]Department of Engineering Science, University of Oxford, Oxford OX1 3PJ, UK.

† Electronic Supplementary Information (ESI) available: Additional Fig.s. See DOI: 10.1039/b000000x/

1 J. Wu and H. Yang, *Acc. Chem. Res*., 2013, **46**, 1848-1857.
2 N. M. Markovic, T. J. Schmidt, V. Stamenkovic and P. N. Ross, *Fuel Cells*, 2001, **1**, 105-116.
3 Y. Bing, H. Liu, L. Zhang, D. Ghosh and J. Zhang, *Chem. Soc. Rev*., 2010, **39**, 2184-2202.
4 Y. Yu, H. Li, H. Wang, X.-Z. Yuan, G. Wang and M. Pan, *J. Power Sources*, 2012, **205**, 10-23.
5 J. C. Meier, C. Galeano, I. Katsounaros, A. A. Topalov, A. Kostka, F. Schu□th and K. J. J. Mayrhofer, *ACS Catal*., 2012, **2**, 832-843.
6 I. E. L. Stephens, A. S. Bondarenko, U. Grønbjerg, J. Rossmeislc and I. Chorkendorff, *Energy Environ. Sci*., 2012, **5**, 6744-6762.
7 H.-W. Liang, W. Wei, Z.-S. Wu, X. Feng and K. Müllen, *J. Am. Chem. Soc*., 2013, **135**, 16002-16005.
8 G. Liu, X. Li, J.-W. Lee and B. N. Popov, *Catal. Sci. Technol*., 2011, **1**, 207-217.
9 P. Chen, T.-Y. Xiao, Y.-H. Qian, S.-S. Li and S.-H. Yu, *Adv. Mater*., 2013, **25**, 3192-3196.
10 L. Qu, Y. Liu, J.-B. Baek and L. Dai, *ACS Nano*, 2010, **3**, 1321-1326.
11 K. Gong, F. Du, Z. Xia, M. Durstock and L. Dai, *Science*, 2009, **323**, 760-764.
12 Z. Wang, R. Jia, J. Zheng, J. Zhao, L. Li, J. Song and Z. Zhu, *ACS Nano*, 2011, **5**, 1677-1684.
13 Z.-H. Sheng, L. Shao, J.-J.Chen, W.-J. Bao, F.-B. Wang and X.-H. Xia, *ACS Nano*, 2011, **5**, 4350-4358.
14 Y. Li, W. Zhou, H. Wang, L. Xie, Y. Liang, F. Wei, J.-C. Idrobo, S. J. Pennycook and H. Dai, *Nat. Nanotechnol*., 2012, **7**, 394-400.
15 H. Peng, Z. Mo, S. Liao, H. Liang, L. Yang, F. Luo, H. Song, Y. Zhong and B. Zhang, *Sci. Rep.,* 2013, **3**, 1765..
16 R. Liu, C. Malotki, L. Arnold, N. Koshino, H. Higashimura, M. Baumgarten and K. Mullen, *J. Am. Chem. Soc*., 2011, **133**, 10372-10375.
17 R. McGuire. Jr., D. K. Dogutan, T. S. Teets, J. Suntivich, Y. Shao-Horn and D. G. Nocera, *Chem. Sci.*, 2010, **1**, 411-414.
18 H. Tang, H. Yin, J. Wang, N. Yang, D. Wang and Z. Tang, *Angew. Chem. Int. Ed*., 2013, **52**, 5585-5589.
19 U. N. Maiti, W. J. Lee, J. M. Lee, Y. Oh, J. Y. Kim, J. E. Kim, J. Shim, T. H. Han and S. O. Kim, *Adv. Mater.*, 2014, **26,** 40-67.
20 D. H. Lee, W. J. Lee, W. J. Lee, S. O. Kim and Y.-H. Kim, *Phys. Rev. Lett.,* 2011, **106,** 175502.
21 R. Jasinski, *Nature*, 1964, **201**, 1212-1213.
22 A. Morozan, S. Campidelli, A. Filoramo, B. Jousselme and S. Palacin, *Carbon*, 2011, **49,** 4839-4847.
23 Q. Liu and J. Zhang, *Langmuir*, 2013, **29**, 3821-3828.
24 W. Li, A. Yu, D. C. Higgins, B. G. Llanos and Z. Chen, *J. Am. Chem. Soc*., 2010, **132**, 17056-17058.
25 Y. Jiang, Y. Lu, X. Lv, D. Han, Q. Zhang, L. Niu and W. Chen, *ACS Catal*., 2013, **3**, 1263-1271.
26 G. Wu, K. L. More, C. M. Johnston and P. Zelenay, *Science*, 2011, **332**, 443-447.
27 X. Fu, Y. Liu, X. Cao, J. Jin, Q. Liu and J. Zhang, *Appl. Catal., B*, **130-131**, 2013, 143-151.
28 C. W. B. Bezerr, L. Zhang, K. Lee, H. Liu, A. L. B. Marques, E. P. Marques, H. Wang and J. Zhang, *Electrochim. Acta*., 2008, **53**, 4937-4951.
29 J. H. Zagal, F. Bedioui and J.-P. Dodelet, in *N_4-macrocyclic metal complexes*, Springer, New York, 2006.
30 D. H. Lee, W. J. Lee, W. J. Lee, S. O. Kim and Y.-H. Kim, *Phys. Rev. Lett*., 2011, **106**, 175502.
31 H. He, Y. Lei, C. Xiao, D. Chu, R. Chen and G. Wang, *J. Phys. Chem. C*, 2012, **116**, 16038-16046.
32 N. Ramaswamy, U. Tylus, Q. Jia and S. Mukerjee, *J. Am. Chem. Soc*., 2013, **135**, 15443-15449.
33 W. Orellana, *J. Phys. Chem. C*, 2013, **117**, 9812-9818.
34 Y.-J. Wang, D. P. Wilkinson and J. Zhang, *Chem. Rev*., 2011, **111**, 7625-7651.
35 S. Sharma and B. G. Pollet, *J. Power Sources*, 2012, **208**, 96-119.
36 Y. Liu, T. G. Kelly, J. G. Chen and W. E. Mustain, *ACS Catal*., 2013, **3**, 1184-1194.
37 E. Antolini and E. R. Gonzalez, *Appl. Catal., B*, 2010, **96**, 245-266.
38 R. B. Levy and M. Boudart, *Science*, 1973, **181**, 547-549.
39 Z. Yan, M. Cai and P. K. Shen, *Sci. Rep*., 2013, **3**, 1646.
40 X, Zhou, Y, Qiu, J. Yu, J. Yin and S. Gao, *Int. J. Hydrogen Energy*, 2011, **36**, 7398-7404.
41 Y. Liu and W. E. Mustain, *ACS Catal*., 2011, **1**, 212-220.
42 S. Yin, M. Cai, C. Wang and P. K. Shen, *Energy Environ. Sci*., 2011, **4**, 558-563.
43 K. Jiang, Q. Jia, M. Xu, D. Wu, L. Yang, G. Yang, L. Chen, G. Wang and X. Yang, *J. Power Sources*, 2012, **219**, 249-252.
44 A-R. Ko, S.-B. Han, Y.-W. Lee and K.-Y. Park, *Phys. Chem. Chem. Phys*., 2011, **13**, 12705-12707.
45 V. Baskin and L. Meyer, *Phys. Rev*., 1955, **100**, 544.
46 M.S. Dresselhaus, G. Dresselhaus, R. Saito and A. Jorio, *Phys. Rep*., 2005, **409**, 47-99.
47 Y. Shao, S. Zhang, M. H. Engelhard, G. Li, G. Shao, Y. Wang, J. Liu, I. A. Aksayc and Y. Lin, *J. Mater. Chem*., 2010, **2**0, 7491-7496.
48 A. T. Garcia-Esparza, D. Cha, Y. Ou, J. Kubota, K. Domen and K. Takanabe, *ChemSusChem*, 2013, **6**, 168-181.
49 C. Zhang, R. Hao, H. Liao and Y. Hou, *Nano Energy*, 2013, **2**, 88-97.
50 K. Artyushkova, B. Kiefer, B. Halevi, A. Knop-Gericke, R. Schlogl and P. Atanassov, *Chem. Commun.,* 2013, **49**, 2539-2541.

51 J. F. Moulder, W. F. Stickle, P. E. Sobel and K. D. Bomben, in *Handbook of X-ray Photoelectron Spectroscopy,* Physical Electronics, Inc., Minnesota, 1995.
52 S. Pylypenko, S. Mukherjee, T. S. Olson and P. Atanassov, *Electrochim. Acta*, 2008, **53**, 7875-7883.
53 M. S. Thorum, J. M. Hankett and A. A. Gewirth, *J. Phys. Chem. Lett*., 2011, **2**, 295-298.

Graphical abstract

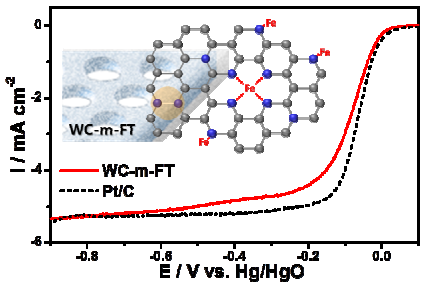

The WC-m-FT shows excellent electrochemical properties in ORR due to iron and nitrogen species as catalytic sites, and mesoporous structure.